

한국표면공학회지  
Journal of the Korean Institute of Surface Engineering  
Vol. 34, No. 5, Oct. 2001  
< 연구논문 >

## Heat Treatment Effects on the Phase Evolutions of Partially Stabilized Grade Zirconia Plasma Sprayed Coatings

Han-Shin Choi, Hyung-Jun Kim\*, Chang-Hee Lee

*Division of Material Science and Engineering, Hanyang University,  
Seoul 133-791, South Korea*

*\*RIST, Welding & Structural Integrity Research Team, Pohang 790-600,  
South Korea CAPST*

### Abstract

Partially stabilized zirconia (PSZ) is an attractive material for thermal barrier coating. Zirconia exists in three crystallographic phases: cubic, tetragonal and monoclinic. Especially, the phase transformation of tetragonal phase to monoclinic phase accompanies significant volume expansion, so this transition generally results in cracking and contributes to the failure of the TBC system. Both the plasma sprayed  $ZrO_2-8Y_2O_3$  (YSZ) coat and the  $ZrO_2-25CeO_2-2.5Y_2O_3$  (CYSZ) coat are isothermally heat-treated at 1300°C and 1500°C for 100hr and cooled at different cooling rates. The monoclinic phase is not discovered in all the CYSZ annealed at 1300°C and 1500°C. In the 1500°C heat-treated specimens, the YSZ contains some monoclinic phase while none exists in the 1300°C heat-treated YSZ coat. For the YSZ, the different phase transformation behaviors at the two temperatures are due to the stabilizer concentration of high temperature phases and grain growth. For the YSZ with 1500°C-100hr annealing, the amount of monoclinic phase increased with the slower cooling rate. The extra oxygen vacancy, thermal stress, and c to t' phase transformation might suppress the t to m martensitic phase transformation.

### 1. Introduction

The performance of a thermal barrier coating (TBC) can be improved by the elucidation of the failure mechanism. And there are many factors limiting the lifetime of the TBC system such as thermally activated processes (creep, oxidation of the bond coat and sintering), stress evolution (thermal expansion mismatch stress and phase transformation) and so on.<sup>1-3)</sup> These factors contribute to fail the coating system simultaneously so it is difficult to separate a respective contribution due to the dynamic responses of the coating

system to the high temperature environment.

Thermal efficiencies of gas turbine engines can be increased by the further increase of the inlet temperature. And, thus, the phase stability of thermal barrier coatings in high temperature is the key point to increase the thermal efficiency of gas turbine engine system.<sup>4-6)</sup> As raising the exposure temperature accelerates diffusion rate, stabilizing elements redistribution and resultant phase separation and transformation become critical during heat treatments. In principle, during cooling tetragonal to monoclinic martensitic phase transformation accompanies 3-5 % volume

expansion. And, thus, this kind of transformation deteriorates the integrity of thermal barrier coatings. Therefore, long-term phase stability and phase evolutions of APS TBCs must be elucidated in order to allow them to be used for a further increased temperature.

In this study, phase evolutions of APS yttria stabilized zirconia (YSZ) and ceria and yttria stabilized zirconia (CYSZ) coatings were observed according to heat treatments.

## 2. Experimental Procedure

Chemical compositions of spraying materials are shown in Table 1. Zirconia solid solutions were deposited onto the grit-blasted mild steel using atmospheric plasma spraying process. Nitrogen and hydrogen gas were used as a 1<sup>st</sup> plasma gas and a 2<sup>nd</sup> one, respectively. The other process parameters were shown in Table 2. Free-standing specimens were made by removing steel substrate using a chemical etching and the specimen dimension was 10×10×1 mm. The specimens were isothermally heated at 1300°C and 1500°C for 100hr, and then cooled to room temperature at four different cooling rates: water quenching, air cooling, and furnace cooling. The phase fractions were identified by using X-ray diffractometer and calculated using Toraya formulae<sup>7)</sup> (XRD, 40kV, 100mA, Cu K $\alpha$  radiation). And Vickers and Knoop indentation tests were carried out under the 300 g

Table 2 Parameters for plasma spraying

| Coating Materials   | Ampere (A) | Voltage (V) | Primary Gas         | Secondary Gas      | Carrier Gas        | Feed Rate (g/min) | Spray Distance (mm) |
|---|------------|-------------|---------------------|--------------------|--------------------|-------------------|---------------------|
|   |            |             | N <sub>2</sub> SCFH | H <sub>2</sub> FMR | N <sub>2</sub> FMR |                   |                     |
| ZrO <sub>2</sub> -CeO <sub>2</sub> -Y <sub>2</sub> O <sub>3</sub> | 500        | 76          | 100                 | 20                 | 12                 | 45                | 100                 |
| ZrO <sub>2</sub> -Y <sub>2</sub> O <sub>3</sub>                   | 500        | 76          | 100                 | 20                 | 12                 | 45                | 100                 |

Table 1. Characteristics of powders

| Powder                         | ZrO <sub>2</sub> -CeO <sub>2</sub> -Y <sub>2</sub> O <sub>3</sub>      | ZrO <sub>2</sub> -Y <sub>2</sub> O <sub>3</sub>  |
|--------------------------------|--|--|
| Chemical Composition (wt.%)    | ZrO <sub>2</sub> -25CeO <sub>2</sub> -2.5Y <sub>2</sub> O <sub>3</sub> | ZrO <sub>2</sub> -8Y <sub>2</sub> O <sub>3</sub> |
| Particle Shape                 | Spheroidal   | Spheroidal                                       |
| Particle Size Range ( $\mu$ m) | -90+16 $\mu$ m   | -106+11 $\mu$ m                                  |

load and a 15 s loading-unloading cycle, and at least 20 tests were performed on each specimen considering specimen geometry and indentation size effect (ISE)<sup>8)</sup>. In order to measure the grain size, both as-sprayed and aged specimens were polished to a 1 $\mu$ m diamond finish and thermally etched at 1400°C for 16m. And then the grain size distribution and average grain size were measured by image analysis.

## 3. Results and Discussion

### 3.1 As-sprayed coatings

Fig. 1 shows the cross-sectional morphology of an as-sprayed APS coating. This is a typical lame-

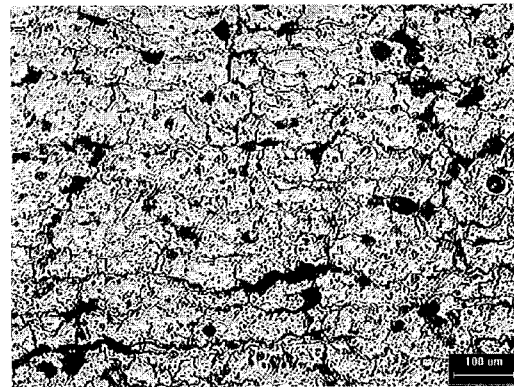


Fig. 1 Cross-sectional morphology of an as-sprayed thermal barrier coating

llar structure of thermal spraying coating containing pore and crack. These defect-like structures contribute to lower thermal conductivity and elastic modulus. In reality, the elastic modulus of as-sprayed YSZ coating was 20.7 GPa measured by knoop indentation method<sup>9)</sup> (load=300gf, a loading-unloading time=15s, elastic recovery (H/E)=0.08). This is far lower value than a sintered one.

APS YSZ coating consisted of a non-transformable tetragonal phase ( $t'$ ), as shown in Fig. 2 (a).  $t'$  is a non-equilibrium phase in which stabilizing element is supersaturated due to splat quenching effect; that is an intrinsic process of thermal spraying.<sup>10)</sup> The addition of trivalent oxide to zirconia results in the reduction of tetragonality. And, thus, the tetragonal symmetry can be retained to room temperature. On the other hand, APS CYSZ coating consisted of  $t'$  and cubic phase (Fig. 2 (b)). The presence of cubic phase partially might be due to unmelted particles and the inhomogeneity of feeding stock materials confirmed the presence of cerium-rich splats. In addition,

the partial reduction of tetravalent Ce cation to trivalent one<sup>11)</sup> occurred due to the reducing environment in  $N_2-H_2$  plasma jet. This is indirectly observed by the change of color. And it could be confirmed by x-ray photoelectron spectroscopy, as shown in Fig. 3. Cerium 3d spectra spectroscopy, as shown in Fig. 3. Cerium 3d spectra was measured using monochromated Al  $K\alpha$  x-ray source (350W). And the peak shift due to the charging effect was calibrated using C 1s peak (BE=284.6 eV). The formation of  $Ce^{+3}$  implies the existence of oxygen vacancy that acts as a cubic phase stabilizer in zirconia solid solutions.

### 3. 2 Isothermal heat-treated at 1300°C

Fig. 4 shows the cross-sectional morphology after ageing for 100h at 1300°C. Densification through healing micropore and microcrack occurred and resultant increases of micro-hardness and elastic modulus were also observed (YSZ: E = 28.8 GPa, H/E = 0.069).

In the case of YSZ coating, the phase composition of aged YSZ consisted of cubic phase and

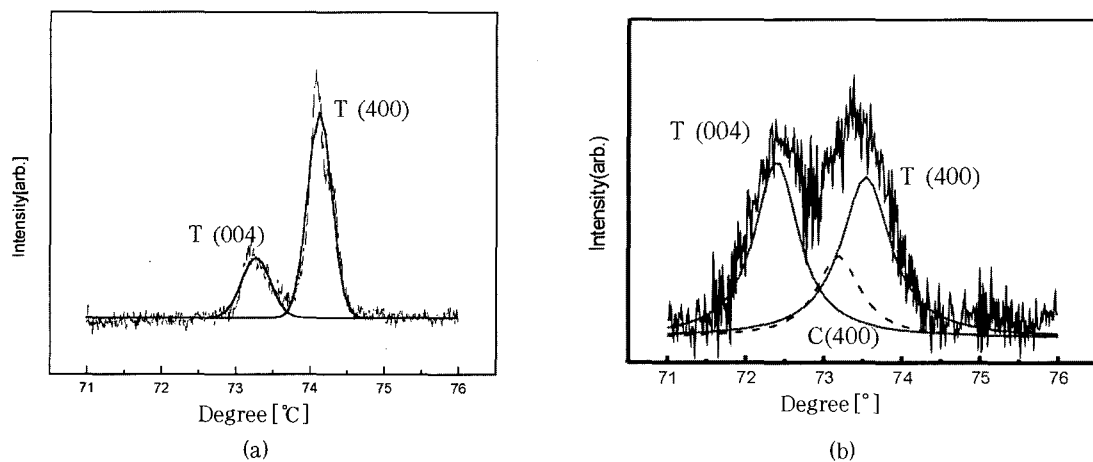


Fig. 2 XRD patterns of as-sprayed state  
(a) YSZ (b) CYSZ

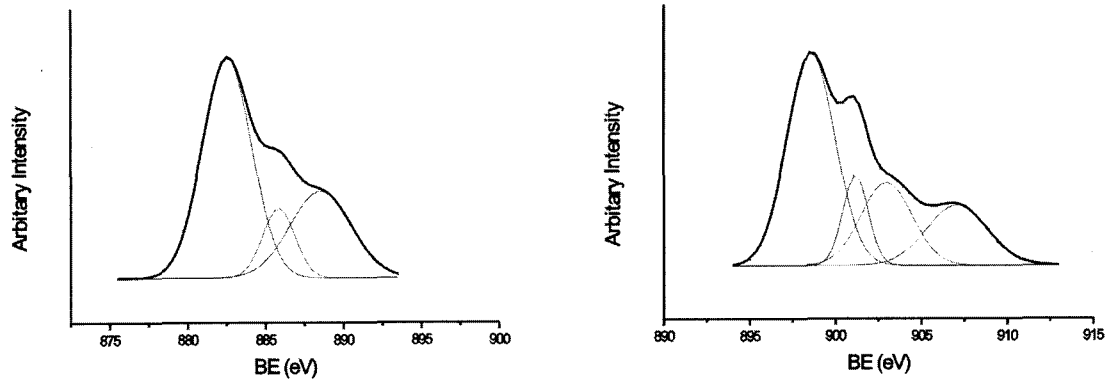


Fig. 3 Cerium 3d spectra on a coating

|                  | Ce 3d <sub>5/2</sub> | Ce 3d <sub>3/2</sub> |
|------------------|----------------------|----------------------|
| Ce <sup>+4</sup> | 882.1, 888.4, 898.1  | 900.6, 907.1         |
| Ce <sup>+3</sup> | 885.3                | 903.8                |

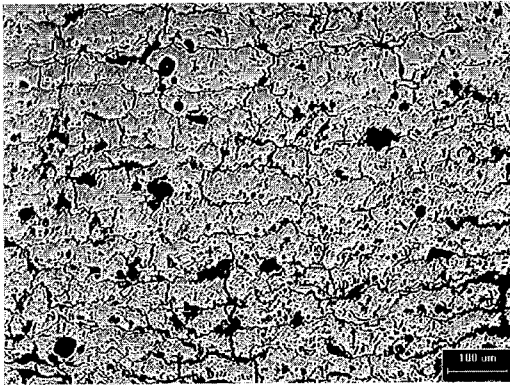


Fig. 4 Cross-sectional morphology of an 1300°C-100h aged thermal barrier coating

tetragonal phase. There was no t to m martensitic phase transformation, regardless of cooling rates. During ageing at 1300°C, phase transition from non-equilibrium t' single phase to equilibrium t and c phase mixture due to the diffusion of stabilizing element. Newly formed tetragonal phase has lower contents of stabilizing element than t', and this t phase is regarded as a transformable t. Nevertheless, t to m martensitic phase transformation could not be observed. T to m martensitic phase transformation depends on various factors,

such as chemical composition, grain size, and matrix constraint. As the stabilizing elements contents increases, Ms temperature decreases. In fact, t phase formed at 1300°C has relatively higher contents of stabilizing elements, and it increases the phase stability of t phase. Grain size of transformable tetragonal phase is another factor affecting the t to m martensitic phase transformation. It is known to be grain size criteria concerning t to m phase transition; critical grain size and minimum grain size. Grain growth increases the driving force for t to m martensitic phase transformation. If grain size of t phase is above the critical grain size, t phase will spontaneously transform to m phase during cooling. However, stress induced martensitic phase transformation will occur when the external stress is applied if the grain size is lying between a minimum size and a critical size. Otherwise, t phase having a lower grain size than a minimum size can be retained at RT. The grain size measurement and indentation test were executed to evaluate the grain size effects. The average grain size was

about  $0.77\mu\text{m}$  and it has a bimodal grain size distribution, as shown in Fig. 5. According to Winnubst et al.<sup>12)</sup>, the minimum grain size of 4.5 wt.%  $\text{Y}_2\text{O}_3$  stabilized zirconia is  $0.25\mu\text{m}$ . However, there was no stress induced martensitic phase transformation before and after indentation, as shown in Raman spectra (Fig. 6). Through this, the grain size of newly formed t phase may be lower than  $0.25\mu\text{m}$  in this condition. And also the increase of elastic modulus increased the matrix constraint and, thus, partially it increase of t phase stability. The existence of cubic phase in coating seemed to be due to the c phase chemistry concerning the c-t'

phase boundary.<sup>13)</sup>

In the case of CYSZ coating, similar behaviors to YSZ coating were observed.

### 3. 3 Isothermal heat-treated at $1500^\circ\text{C}$

Fig. 7 shows the cross-section of aged APS TBC at  $1500^\circ\text{C}$  for 100 h. High temperature activated sintering and densification resulted in dense and stiff coating. The elastic modulus of YSZ coating was about 40 GPa.

In the case of YSZ coating, the average grain size was  $1.30\mu\text{m}$ , and bimodal grain size distribution generally shifted to larger grain size, as

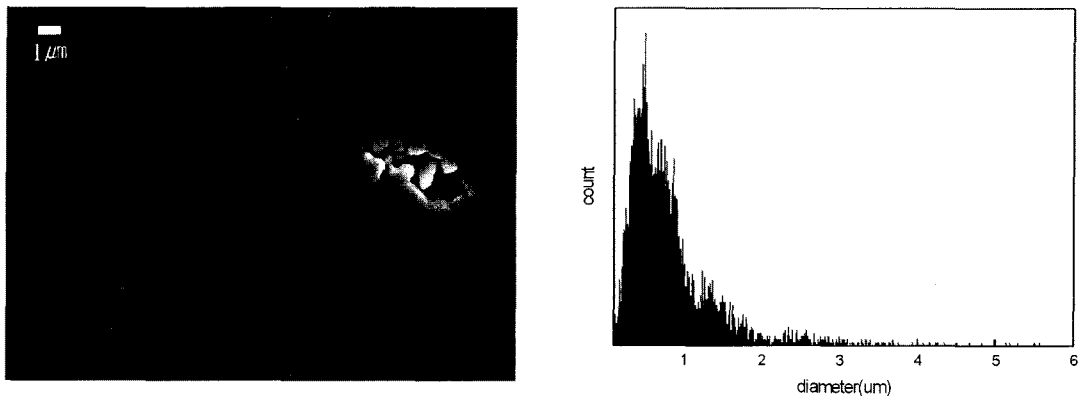


Fig. 5 Plane-view morphology and grain size distribution of YSZ coating ( $1300^\circ\text{C}$ -100h)

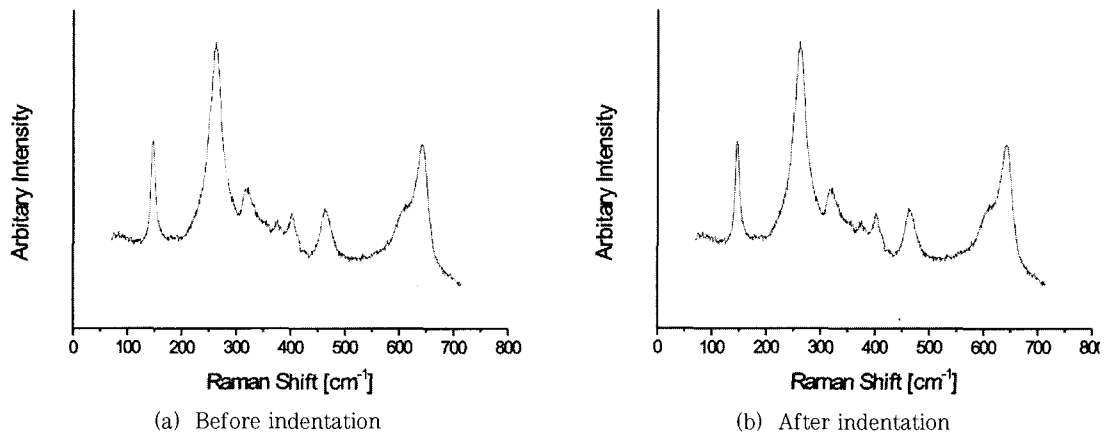


Fig. 6 Raman spectra of YSZ coating ( $1300^\circ\text{C}$ -100h)

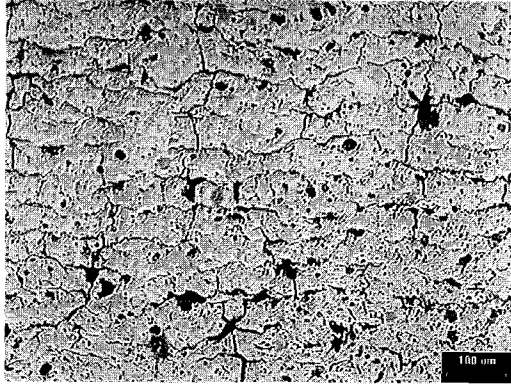


Fig. 7 Cross-sectional morphology of an 1500°C-100h aged thermal barrier coating

shown in Fig. 8. It was observed that *t* to *m* martensitic phase transformation highly depended on the cooling rate, as summarized in Fig. 9. As the cooling rate was increased, the *t* to *m* martensitic phase transformation was suppressed but the *c* to *t'* diffusionless transformation was increased. As can be expected in  $ZrO_2$ - $Y_2O_3$  phase diagram, equilibrium *t* and *c* phase separated at 1500 °C has relatively lower stabilizing element and larger grain size. And, thus, the driving force of *t* to *m* martensitic phase transformation seemed to be increased though the matrix constraint became larger due to the densification.

Fig. 10 shows the Raman spectra of static-air cooled specimen before and after indentation. When the external load was applied, the retained *t* phase transformed to *m* phase including *t* phase having between minimum and critical grain size range. The effects of cooling rate on the suppression of *t* to *m* martensitic phase transformation are under intensive studies. Partially it might result from thermal stress, oxygen vacancy, and *c* to *t'* phase transformation.

Fig. 11 shows the phase composition of CYSZ according to heat treatments. In the case of CYSZ

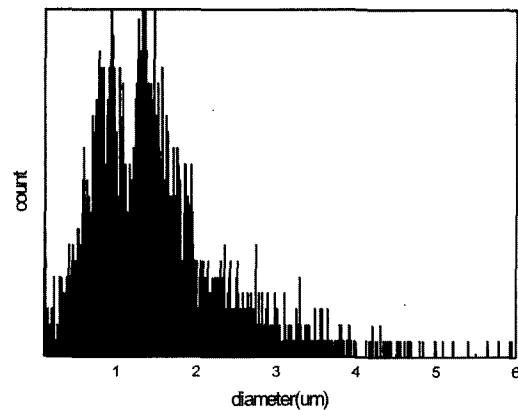
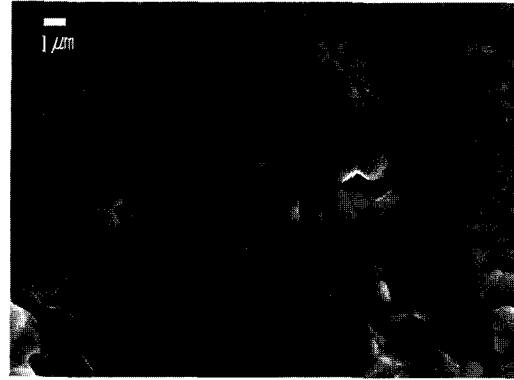


Fig. 8 Plane-view morphology and grain size distribution of YSZ coating (1500°C-100h)

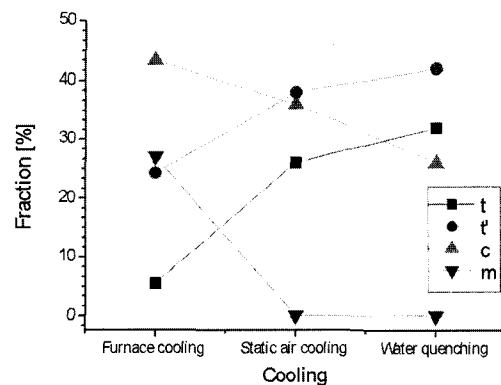


Fig. 9 Phase composition of YSZ coatings according to heat treatments

coating, high stabilizer containing *t'* phase fraction decreased while low stabilizer containing *t* phase fraction increased due to the diffusion of

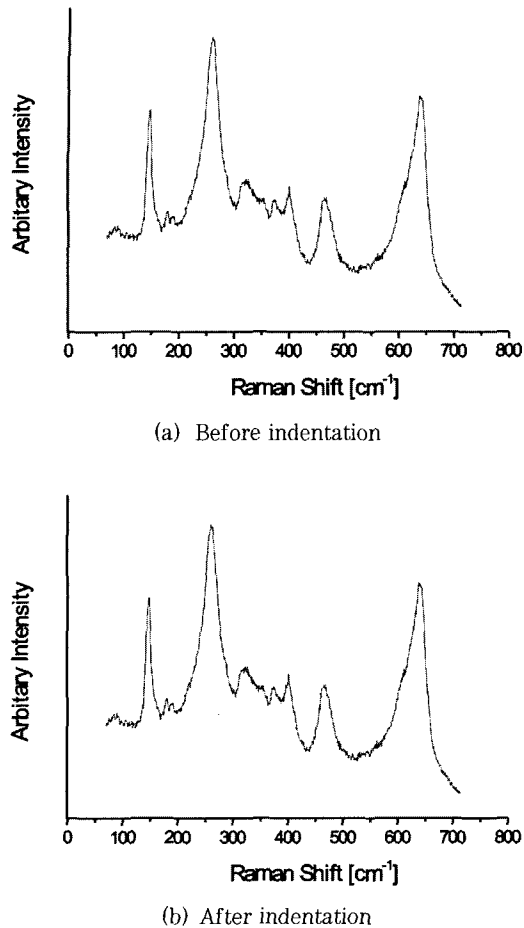


Fig. 10 Raman spectra of YSZ coating (1500°C-100h)

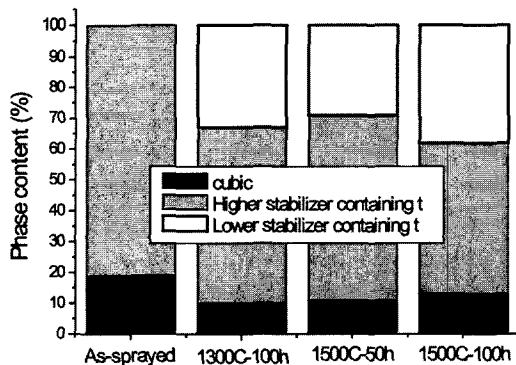


Fig. 11 Phase composition of CYSZ coatings according to heat treatments

stabilizing element during ageing. And the decrease of cubic phase fraction might result from the reoxidation of  $Ce^{3+}$  to  $Ce^{4+}$  because of the annihilation of oxygen vacancy, cubic phase stabilizer. To the contrary to YSZ coating, there was no t to m martensitic phase transformation, regardless of cooling rates. This implies that the stabilizer content in the stable t formed by the thermally activated process may be high enough to stabilize the t phase to the room temperature as can be seen in  $ZrO_2$ - $CeO_2$  phase diagram. In other words, the CYSZ is more stable than YSZ because of the initial chemical composition. The  $Y^{+3}$  ion in the YSZ and the  $Ce^{+4}$  ion in CYSZ are major cations, and  $Ce^{+4}$  ionic radius (1.01 Å) is larger than  $Y^{+3}$  ionic radius (0.92 Å). Therefore, during high temperature aging, the YSZ is easily decomposed into transformable tetragonal phase and cubic phase, compared with CYSZ. The transformable tetragonal phase containing low stabilizer can transform to monoclinic phase on cooling. From the viewpoint of phase equilibrium, it can be concluded that  $CeO_2$  provided partial stabilization of  $ZrO_2$  over a wide range of composition<sup>10</sup>. And the long term phase stability and exact reasons why thermally decomposed stable t did not undergo the martensitic phase transformation is under intensive investigations.

## Conclusion

The phase evolutions of atmospheric plasma sprayed thermal barrier coatings were evaluated according to chemical composition and heat treatments. CYSZ coating shows the higher thermal stability than YSZ one at high temperature. This may be due to the high stabilizing elements

contents enough to reduce the Ms temperature below room temperature. Spontaneous t to m martensitic phase transformation was observed in YSZ coating that was aged at 1500°C for 100h and cooled to room temperature through furnace cooling. The suppression effects of fast cooling may be due to the conjugated effects of thermal stress, oxygen vacancy, and c to t' phase transformation.

### Acknowledgement

This study was supported from the CAPST (ERC program, KOSEF)

### References

1. J. R. VanValzah, H. E. Eaton, *Surface and Coatings Technology*, 46, 289 (1991)
2. J.R. Brandon and R. Taylor, *Surface and Coatings Technology*, 46, 75 (1991)
3. C. H. Lee, H. K. Kim, H. S. Choi, H. S. Ahn, *Surface & Coatings Technology* 124, 1 (2000)
4. S. H. Lee, J. S. Yoo, J. Y. Kim, C. S. Kang, *J. of the Korean Inst. of Met. & Mater.*, 35 1744 (1997)
5. A. Bennett, F. C. Toriz, A. B. Thakker, *Surface and Coatings Technology*, 32, 359 (1987)
6. R. A. Miller, *Surface and Coatings Technology*, 30, 1 (1986)
7. Hideo Toraya, Masahiro Yoshimura, *Journal of American Ceramic Society*, C-119 (1984)
8. J. B. Quinn, G. D. Quinn, *Journal of Materials Science*, 32, 4331 (1997)
9. D. B. Marshall, T. Noma, A. G. Evans, *Journal of the American Ceramic Society*, 65, C175 (1982)
10. A.H. Heuer, R. Chaim and V. Lanteri, *Science and Technology III* (The American Ceramic Society, 1988)
11. R. D. Maschio, P. Scardi, L. Lutterotti, *Journal of Materials Science* 27, 5591 (1992)
12. A. J. A. Winnubst, A. J. Burggraaf, *Advanced in Ceramics Vol. 24A Science and Technology of Zirconia III*, 39 (1988)
13. M. Yashima, H. Arashi, M. Kakihana, M. Yoshimura, *Journal of the American Ceramic Society*, 77 1067 (1994)